Transoid, Ortho, and Gauche Conformers of *n*-Si_4Cl_{10}: Raman and Mid-IR Matrix-Isolation Spectra†

Robert Zink, Thomas F. Magnera, and Josef Michl*

Department of Chemistry and Biochemistry, University of Colorado, Boulder, Colorado 80309-0215

Received: November 12, 1999; In Final Form: January 31, 2000

Calculations at the HF/6-31G*, MP2(FC)/6-31G*, and B3LYP/6-31G* levels of theory predict the existence of three pairs of enantiomeric conformers on the potential energy surface of *n*-Si_4Cl_{10}: transoid, ortho, and gauche. At the fully optimized MP2(FC)/6-31G* level the SiSiSiSi dihedral angles (deg) and relative energies (kcal/mol) are 160.5° and 0.0 (transoid), 93.0° and 0.65 (ortho), and 48.7° and 0.27 (gauche). Matrix annealing, spectral differencing, and singular value decomposition analyses of Raman and mid-IR spectra of *n*-Si_4Cl_{10} in nitrogen matrix demonstrate that three distinct backbone conformers are indeed trapped in the matrices and interconvert upon annealing. Their initial relative concentrations and the details of the annealing behavior depend on the matrix isolation ratio. Their vibrational spectra have been assigned by comparison with results of MP2(FC)/6-31G* calculations and the nature of the normal modes has been analyzed in terms of calculated potential energy distributions. Annealing in concentrated matrices (N_2:*n*-Si_4Cl_{10} ~ 200:1) indicates that at least in some environments, the relative stability of the conformers increases in the order gauche < ortho < transoid, in agreement with results of HF/6-31G* and B3LYP/6-31G* calculations.

Introduction

In the past it was often assumed that the conformational isomerism of all unconstrained, saturated linear A_4X_{10} chains is similar to that familiar from *n*-alkanes, i.e., that there exists a racemic gauche minimum (backbone dihedral angle ϕ about ±60°) and an anti minimum (achiral with $\phi = 180°$ or racemic with ϕ about ±165°, which we would now call transoid). Early very approximate calculations for various chains sometimes predicted the existence of a third backbone conformer with ϕ about ±90°, but at times they also made such predictions for unsubstituted alkanes and oligosilanes, where they are clearly incorrect, and they were generally not regarded as trustworthy.[1]

Subsequent more accurate and less easily dismissed ab initio calculations predicted the existence of a third backbone conformer with ϕ in the vicinity of ±90° (termed ortho[2,3]) for *n*-Si_4Me_{10}[4,5] and *n*-C_4F_{10}.[2,3,6] A general analysis for *n*-A_4X_{10} chains[7] then reached the conclusion that for simple substituents X whose crystallographic van der Waals radius is 0.8−1.0 times the AA bond length, three stable enantiomeric pairs of backbone conformers, anti (now called transoid), ortho, and gauche, will appear on the potential energy surface as a result of an interplay between intrinsic rotational barriers and repulsive van der Waals substituent interactions. Most recently, computational examination of the conformers of Si_4Et_{10},[8] $Si_4Me_8Et_2$,[9] and $Si_4Me_6Et_4$[9] suggested that for longer alkyl chain substituents there will actually be five favored backbone conformations, but there is only very limited experimental evidence for the correctness of this prediction. Nevertheless, anticipating that it will turn out to be right, we have adopted a nomenclature that has been recently proposed[10] for linear backbone conformations: anti ($\phi = 180°$), transoid (~165°), deviant (~145°), ortho (~90°), gauche (~60°), cisoid (~40°), and syn (0°). The only consequence for the present paper is the adoption of the label "transoid" for the conformation that we previously[2−5,7,11−15] called anti.

The existence of three rotamers differing in backbone conformation and their thermal interconversion have been unambiguously proven for the *n*-C_4F_{10} chain by direct observation of mid-IR matrix-isolation spectra.[2,3] In contrast, only two of the three expected conformers of *n*-Si_4Me_{10} were detected by this technique,[5] perhaps not surprisingly, as the mid-IR spectra of the ortho and gauche form were predicted to be virtually identical. A very recent gas-phase electron diffraction study confirmed the presence of the transoid and gauche conformations and concluded that the ortho conformer is probably present as well; density functional calculations gave results very similar to the earlier ab initio ones.[16] A definitive proof of the existence of the ortho conformer in a substituted four-silicon chain has thus remained elusive so far.

We suspected that the vibrational frequencies of the two twisted conformers of a A_4X_{10} chain might differ more when the mass of the substituents X is comparable to that of the backbone atoms A. Since the Cl substituent is similar in size to the methyl group, it is not surprising that three pairs of enantiomeric conformers have been predicted[7] for *n*-Si_4Cl_{10}, and it thus represents an attractive substrate for further testing of the general theoretical result. Indeed, a calculation of its normal-mode frequencies predicted that several deformation mode frequencies will vary more significantly with the conformation of the central SiSi bond than was the case for Si_4Me_{10}, providing some hope that individual peaks of all three conformers could be identified in matrix-isolation spectra. In the present paper, we report the results of these calculations and of a Raman and mid-IR matrix-isolation spectroscopic study of *n*-Si_4Cl_{10} in N_2, which finally provides definitive experimental evidence for the existence of three conformers of a four-silicon chain.

Our interest stems primarily from the fact that an understanding of the conformational properties of tetrasilane chains is

† Part of the special issue "Marilyn Jacox Festschrift".

10.1021/jp994017j CCC: $19.00
Published on Web 03/28/2000

TABLE 1: Computed Properties of the Transoid, Ortho, and Gauche Conformers of *n*-Si_4Cl_{10}

	HF/6-31G*			MP2(FC)/6-31G*			B3LYP/6-31G*		
	transoid	ortho	gauche	transoid	ortho	gauche	transoid	ortho	gauche
total energy (au)	−5751.01512	−5751.01398	−5751.01386	−5752.62418	−5752.62315	−5752.62375	−5760.45308	−5760.45238	−5760.45222
rel energy (kcal mol^{-1})	0.00	0.72	0.79	0.00	0.65	0.27	0.00	0.44	0.54
r(SiSi) (central bond)/Å	2.373	2.382	2.378	2.346	2.354	2.351	2.379	2.388	2.385
r(SiSi) (outer bonds)/Å	2.363	2.362	2.360	2.338	2.338	2.336	2.369	2.369	2.367
r($SiCl_3$)/Å[a]	2.041	2.041	2.041	2.039	2.039	2.039	2.061	2.061	2.061
r($SiCl_2$)/Å[a]	2.056	2.056	2.055	2.052	2.052	2.051	2.074	2.074	2.074
ψ(SiSiSi)/deg	115.7	116.3	118.3	113.2	115.3	116.4	115.5	116.3	118.2
ϕ(SiSiSiSi)/deg	164.6	96.0	55.7	160.5	93.0	48.7	163.9	93.5	57.2
ϕ($SiCl_3$)/deg[b]	−9.6	8.6	−8.0	−12.8	8.7	−8.3	−10.2	8.7	−7.6

[a] Average value. [b] $SiCl_3$ twist, zero at the staggered geometry, and positive for a counterclockwise rotation of the terminal $SiCl_3$ end groups when viewed from a point located on the terminal bond axis outside the molecule.

crucial for the description of the influence of backbone conformation on the electronic properties and near-UV spectra of oligosilanes and polysilanes.[10] In addition, it seemed reasonable and necessary to provide additional experimental evidence for the general validity of the calculated "three-conformer regime" in unconstrained linear A_4X_{10} chains with simple substituents X.

Experimental Section and Methods of Calculation

Materials. *n*-Decachlorotetrasilane[17] was prepared from $ClSiPh_2SiPh_2SiPh_2SiPh_2Cl$.[18] This tetrasilane (10 g) was suspended in benzene (20 mL), a small amount of $AlCl_3$ (∼0.05 g) was added, the mixture was briefly heated to 50 °C, and gaseous HCl was passed through the solution. The reaction was finished after 20 min when no additional HCl gas dissolved and the sharp IR band near 1427 cm^{-1}, characteristic of Si−Ph groups, disappeared. Benzene was then distilled off at reduced pressure and *n*-heptane (70 mL) was added to the residue to precipitate the aluminum salts. Solids were removed by decantation and *n*-heptane was distilled off at reduced pressure. The residual liquid was purified by distillation (bp 65 °C/0.05 mbar), giving 5.4 g (92% yield) of *n*-Si_4Cl_{10}. The purity of the sample was checked by comparison with the reported[17] IR, Raman, and ^{29}Si NMR spectra.

Matrix-Isolation Spectroscopy. An *n*-Si_4Cl_{10} sample was held at 15−25 °C or −20 °C for Raman or mid-IR spectroscopy, respectively, and was evaporated into a stream of dry nitrogen (US Welding, ultrahigh purity). The resulting mixture was deposited at a rate of ∼2.5 mmol h^{-1} on a Ni-plated Cu plate (Raman) or polished CsI window (mid-IR). The deposition targets were mounted on the second stage of a closed-cycle helium refrigerator (Air Products Displex 202) and the temperature of the cold tip was maintained at 11 K during all depositions. The amount of nitrogen deposited was approximately 20 mmol for the Raman and 2.5 mmol for the mid-IR measurements. The matrices were annealed with a resistance foil heater located at the cold tip for ∼30 min at a selected temperature and then recooled to 11 K before further spectral measurements were taken.

Raman spectra were observed with a Spex 1404 0.85 m double monochromator using a liquid nitrogen cooled charge coupled device (CCD) camera. The matrices were excited with the 514.5 nm line of an Ar^+ laser (0.3 W). The spectra were collected through a Kaiser Supernotch Plus notch filter and baseline corrected. The Raman spectrum of solid *n*-Si_4Cl_{10} was obtained at −50 °C by mounting a sealed 1 mm diameter capillary glass tube containing the sample on a copper block equipped with a heater and a thermocouple and cooled with liquid nitrogen. Mid-IR spectra were measured at 1 cm^{-1} resolution with a Nicolet 800 spectrometer employing a wide range liquid nitrogen cooled MCT-B detector. Multiple scans were recorded and baseline corrected.

Calculations. Quantum mechanical calculations were done on an HP S-2200 Exemplar computer using the Gaussian 94 program.[19] Full geometry optimizations and harmonic frequency calculations were done at HF/6-31G*, MP2(FC)/6-31G*, and B3LYP/6-31G* levels of theory (Table 1). The frequencies were computed analytically for HF and DFT, and numerically for MP2, using analytically calculated first derivatives. The vibrational frequencies obtained at the HF and MP2 levels were multiplied by scaling factors of 0.90 and 0.95, respectively, which yield the best overall agreement with experimental frequencies, and these scaled wavenumbers are listed in Tables 2−4. The scaled MP2 frequencies were found to agree most satisfactorily with observed peak positions and have been used throughout the text. As it was not possible to compute Raman intensities of the vibrational modes at the MP2 and B3LYP levels with the programs available to us at present, we used Raman intensities calculated at the HF/6-31G* level everywhere in the tables and figures.

The Asym 40 program[20] was used to transform Cartesian Hessian matrices into symmetry coordinate force fields that were subsequently used for normal coordinate analyses and potential energy distribution analyses employing the standard FG formalism of Wilson.[21] All potential energy distribution values used in the text are those calculated at the MP2 level. Singular value decomposition analyses[22] of spectral data were performed with a program assembled from LAPACK[23] subroutines.

Results

Calculated Structures and Spectra. Geometry optimizations at all levels of theory employed predict the existence of three pairs of enantiomeric backbone conformers on the potential energy surface of *n*-Si_4Cl_{10}, with the SiSiSiSi backbone dihedral angles near ±163° (transoid), ±95° (ortho), and ±55° (gauche). The fully optimized geometries possess C_2 symmetry. Energies and structures of the three conformers are collected in Table 1. As noted before,[7] 1,4-substituent interactions cause the $SiCl_3$ end groups to be twisted in opposite directions in the ortho conformer on the one hand and in the transoid and gauche conformers on the other. All calculations predict that the strongly twisted conformers (ortho and gauche) are only slightly less stable than the transoid conformer (Table 1), and all three backbone conformers can be expected to be present in detectable amounts in room-temperature equilibrium. Tables 2−4 summarize the scaled calculated ab initio and unscaled DFT

TABLE 2: Vibrations of Transoid n-Si_4Cl_{10}

			calculated						observed (matrix)	
			$\tilde{\nu}$ (cm^{-1})						$\tilde{\nu}$ (cm^{-1})	
mode	approx label	sym[a]	HF/ 6-31G*	B3LYP/ 6-31G*	MP2/ 6-31G*	int IR MP2/6-31G* (km mol^{-1})	int Raman HF/6-31G* ($Å^4$ amu^{-1})	MP2/6-31G* PED (%)[b]	mid-IR	Raman
1	SiSiSiSi torsion	a_u	8.8	8.8	15.6	0.0	0.00	$77S_{19}$, $31S_{18}$, $17S_{14}$		
2	$-SiCl_3$ torsion	b_g	18.0	16.7	20.0	0.1	0.02	$104S_{26}$, $65S_{35}$		
3	$-SiCl_3$ torsion	a_u	19.6	17.2	20.6	0.0	0.00	$89S_{18}$, $24S_{19}$		
4	SiSiSi bend	b_u	35.3	33.4	36.6	0.2	0.01	$46S_{35}$, $20S_{26}$		
5	SiSiSi bend	a_g	53.5	51.3	48.8	0.0	0.29	$73S_{10}$, $38S_8$, $12S_{15}$		
6	$SiCl_2$ rock	a_u	64.1	63.5	62.3	1.9	0.01	$64S_{16}$, $47S_{15}$		
7	$SiCl_3$ rock	b_g	70.5	68.7	68.0	0.0	0.03	$66S_{23}$, $35S_{24}$, $25S_{25}$		
8	$SiCl_2$ twist	a_u	71.1	70.2	69.0	0.0	0.13	$88S_{17}$, $21S_{15}$, $18S_{16}$		
9	$SiCl_3$ rock	b_u	88.0	86.4	81.5	6.3	0.12	$76S_{33}$, $47S_{36}$		
10	$SiCl_3$ rock	a_g	100.3	100.2	100.5	0.0	5.9	$51S_8$, $17S_7$		110
11	$SiCl_2$ twist	b_g	105.5	105.2	104.8	0.2	5.3	$60S_{25}$, $21S_{23}$, $14S_{22}$		110
12	$SiCl_2$ wag	a_g	113.7	114.8	113.1	0.0	4.0	$57S_{11}$, $13S_6$, $12S_4$		119
13	$SiCl_2$ scissoring	b_u	124.7	125.8	125.2	0.1	0.45	$29S_{34}$, $16S_{31}$, $14S_{30}$, $12S_{36}$, $11S_{32}$		131
14	$SiCl_2$ scissoring	a_g	127.9	128.8	128.6	0.0	5.3	$69S_9$		134
15	$SiCl_3$ rock	a_u	135.6	136.1	136.2	1.5	0.21	$44S_{14}$, $24S_{15}$, $13S_{16}$, $11S_{17}$		134
16	$SiCl_3$ asym def	b_g	165.6	167.5	166.4	3.5	0.43	$45S_{22}$, $21S_{24}$, $17S_{32}$		167
17	$SiCl_3$ asym def	b_u	174.6	177.0	175.2	17.5	1.0	$59S_{32}$, $15S_{34}$, $14S_{22}$		177
18	$SiCl_3$ asym def	a_g	182.5	185.5	184.6	0.2	3.9	$72S_7$		188, 187[c]
19	$SiCl_3$ asym def	a_u	195.7	198.7	198.5	3.1	1.8	$51S_{14}$, $10S_{15}$		199
20	$SiCl_3$ sym def	b_u	200.0	203.5	202.0	31.9	1.6	$37S_{34}$, $32S_{31}$		199
21	$SiCl_2$ rock	b_g	210.9	213.9	215.1	5.1	5.9	$34S_{24}$, $15S_{22}$		214
22	$SiCl_2$ wag	b_u	234.6	238.5	237.1	87.2	0.35	$35S_{36}$, $30S_{31}$		
23	$SiCl_3$ sym def	a_g	238.9	242.7	240.4	1.2	1.8	$39S_6$, $19S_{10}$, $12S_9$, $11S_{11}$		241
24	$SiCl_2$ sym stretch	a_g	304.8	306.9	314.7	0.3	32.6	$21S_3$, $18S_1$, $18S_4$, $16S_6$, $14S_5$		318
25	$SiCl_3$ sym stretch	b_u	356.9	358.3	365.9	43.4	0.02	$50S_{27}$, $31S_{30}$		373
26	$SiCl_3$ sym stretch	a_g	429.6	435.6	441.1	4.3	3.8	$60S_1$, $23S_3$, $12S_{11}$, $11S_5$		444
27	$SiCl_2$ sym stretch	b_u	474.6	486.2	491.2	198.3	0.00	$70S_{29}$, $26S_{27}$	490, 488[c]	
28	SiSi stretch	a_g	557.4	564.1	574.5	2.8	3.9	$39S_5$, $28S_3$, $17S_{13}$		571
29	SiSi stretch	b_u	559.8	570.4	577.5	37.4	0.31	$26S_{30}$, $23S_{28}$, $20S_{21}$, $15S_{27}$	574	571
30	$SiCl_2$ asym stretch	b_g	551.1	567.0	582.4	26.9	7.3	$84S_{21}$, $10S_{24}$	585	582
31	$SiCl_2$ asym stretch	a_u	552.9	572.2	583.8	1.6	1.9	$54S_{13}$, $33S_{12}$		582
32	$SiCl_3$ asym stretch	b_g	571.9	587.3	596.5	13.2	4.5	$79S_{20}$, $22S_{28}$	593, 601?	600
33	$SiCl_3$ asym stretch	a_g	573.3	588.5	596.6	7.2	12.3	$82S_2$, $12S_{12}$	593, 601?	600
34	$SiCl_3$ asym stretch	b_u	578.9	593.2	603.5	304.5	0.6	$54S_{28}$, $15S_{30}$, $13S_{20}$	606−608	606
35	$SiCl_3$ asym stretch	a_u	579.2	595.2	604.8	401.1	1.5	$49S_{12}$, $29S_{13}$, $12S_2$	606−608	606
36	SiSi stretch	a_g	588.6	599.5	609.9	40.7	15.0	$42S_4$, $20S_1$, $19S_3$	608−620	617, 618[c]

[a] The u and g symmetry species used are those for the hypothetical anti geometry (planar backbone). [b] Only values larger than 10% are listed. [c] Difference peak.

vibrational frequencies, the calculated IR (MP2) and Raman (HF) intensities, the classification of the calculated normal modes in terms of symmetry coordinates according to the calculated potential energy distributions, and a tentative assignment of calculated to observed modes. The symmetry coordinates chosen are listed in Table 5, using internal coordinates defined in Figure 1.

The Raman vibrations can be divided into stretching modes between 300 and 620 cm^{-1} and deformation modes below 250 cm^{-1}. The predicted mid-IR spectrum can be divided into three main spectral regions. The region between 570 and 620 cm^{-1} is due to asymmetric SiCl and SiSi stretching modes, a narrow spectral region around 490 cm^{-1} is attributed to the $\nu_{sym}(SiCl_2(b))$ mode, and a single peak at ~444 cm^{-1}, ascribed to the $\nu_{sym}(SiCl_3(a))$ mode, should be strong for the twisted conformers but extremely weak for the transoid rotamer.

Next, we describe the vibrational spectra of matrix-isolated conformer mixtures as deposited and their variation upon annealing followed by recooling to 11 K for spectral measurements. The smaller among the spectral effects are attributable to changes in matrix site occupancies while those that involve larger frequency shifts and dramatic changes in intensities are assigned to conformer interconversion. We start with a qualitative analysis of the Raman spectra that strongly suggests that three distinct species are present and possess the vibrational properties predicted for the transoid, ortho, and gauche conformers. Then, we briefly discuss mid-IR matrix-isolation spectra, from which less information about the conformational composition can be extracted. Subsequently, we describe a quantitative treatment that proves beyond reasonable doubt that three conformers are indeed present.

Qualitative Aspects of Observed Spectra. Information on the Raman and IR spectra of n-Si_4Cl_{10} is collected in Table 6.

Raman. Representative spectra are shown in Figures 2−4. According to the calculations (Tables 2−4), the Raman-active vibrations located above 300 cm^{-1} and attributed to stretching modes are not expected to vary much with the backbone conformation and offer little chance to extract useful information about conformational isomerism. This spectral region is dominated by a strong peak at ~318 cm^{-1}, ascribed to the $\nu_{sym}(SiCl_2(a))$ mode, followed by peaks of medium intensity, one near 444 cm^{-1} assigned to $\nu_{sym}(SiCl_3(a))$ and several between 570 and 620 cm^{-1}, attributed to SiSi and asymmetric SiCl stretching vibrations. Very weak peaks appear at ~373

TABLE 3: Vibrations of Ortho *n*-Si_4Cl_{10}

			calculated						observed (matrix)	
			$\tilde{\nu}$ (cm^{-1})						$\tilde{\nu}$ (cm^{-1})	
mode	approximate label	sym	HF/ 6-31G*	B3LYP/ 6-31G*	MP2/ 6-31G*	int IR MP2/6-31G* (km mol^{-1})	int Raman HF/6-31G* (Å^4 amu^{-1})	MP2/6-31G* PED (%)[a]	mid-IR	Raman
1	SiSiSiSi torsion	a	13.3	12.3	14.8	0.0	0.02	$156S_{19}$, $65S_{10}$		
2	$-SiCl_3$ torsion	a	19.2	17.6	23.2	0.0	0.02	$93S_{18}$, $44S_{19}$		
3	$-SiCl_3$ torsion	b	23.3	19.5	24.9	0.0	0.01	$112S_{26}$		
4	SiSiSi bend	b	42.7	40.2	39.2	0.4	0.01	$93S_{35}$, $27S_{33}$, $11S_{23}$		
5	SiSiSi bend	a	44.9	42.0	46.3	0.2	0.09	$61S_{10}$, $11S_{16}$		
6	$SiCl_3$ rock	b	62.9	62.9	58.9	1.5	0.01	$79S_{23}$, $48S_{24}$, $18S_{25}$		
7	$SiCl_3$ rock	a	71.1	69.7	68.9	1.0	0.13	$59S_{15}$, $43S_{16}$, $15S_8$, $12S_{17}$		
8	$SiCl_3$ rock	b	82.9	79.7	75.7	4.0	0.26	$48S_{33}$, $55S_{25}$, $25S_{36}$, $19S_{24}$		
9	$SiCl_3$ rock	a	89.8	88.8	85.7	0.1	0.45	$47S_8$, $47S_{17}$, $16S_{11}$		
10	$SiCl_2$ twist	b	105.9	104.8	104.9	0.6	3.8	$25S_{25}$, $15S_{33}$, $12S_{36}$		110
11	$SiCl_2$ twist	a	104.9	106.0	105.0	0.3	6.6	$27S_{17}$, $18S_8$		110
12	$SiCl_2$ wag	a	113.5	113.5	111.7	0.06	2.6	$51S_{11}$, $12S_5$		119
13	$SiCl_2$ wag	b	123.3	124.5	123.2	0.0	4.7	$33S_{34}$, $14S_{31}$, $13S_{30}$, $12S_{32}$, $12S_{36}$		131
14	$SiCl_2$ scissoring	a	126.6	127.6	128.0	0.0	2.0	$47S_9$, $15S_6$, $13S_4$		134
15	$SiCl_2$ rock	b	148.0	148.2	147.5	3.8	0.01	$46S_{22}$, $21S_{24}$, $12S_{23}$		
16	$SiCl_2$ rock	a	146.2	148.5	148.2	3.0	3.0	$37S_{14}$, $25S_{16}$, $13S_9$, $13S_{15}$		147
17	$SiCl_3$ asym def	b	174.0	176.6	174.7	15.8	0.03	$70S_{32}$, $23S_{34}$		
18	$SiCl_3$ asym def	a	183.8	186.6	186.1	1.7	4.0	$70S_7$		188,190[b]
19	$SiCl_3$ asym def	b	196.5	199.5	199.4	0.7	2.5	$42S_{22}$		199
20	$SiCl_3$ asym def	a	196.7	199.9	199.8	0.0	5.0	$46S_{14}$, $12S_{15}$		199
21	$SiCl_2$ scissoring	b	223.7	227.6	226.7	4.2	1.2	$20S_{34}$, $16S_{35}$		226
22	$SiCl_3$ sym def	a	231.3	234.3	232.2	17.7	2.5	$33S_6$, $16S_{10}$, $14S_9$, $12S_{16}$		235
23	$SiCl_3$ sym def	b	236.4	240.2	238.4	91.5	0.82	$50S_{31}$, $41S_{36}$		241
24	$SiCl_2$ sym stretch	a	303.6	305.7	312.2	6.9	31.8	$19S_4$, $19S_6$, $18S_1$, $18S_3$, $14S_5$		318
25	$SiCl_3$ sym stretch	b	361.8	363.7	372.0	51.5	0.01	$51S_{27}$, $27S_{30}$, $12S_{36}$		373
26	$SiCl_3$ sym stretch	a	427.7	434.4	441.0	73.5	1.9	$57S_1$, $22S_3$, $13S_5$	444	444
27	$SiCl_2$ sym stretch	b	472.5	483.1	488.1	91.3	0.34	$72S_{29}$, $26S_{27}$	493	490
28	SiSi stretch	a	562.5	558.4	568.6	0.1	9.3	$35S_{13}$, $31S_5$, $21S_3$		571
29	$SiCl_2$ asym stretch	b	550.5	566.3	576.6	20.4	0.88	$78S_{21}$, $17S_{28}$	574	571
30	$SiCl_2$ asym stretch	a	546.3	576.4	586.8	47.4	5.7	$55S_{13}$, $17S_5$, $15S_3$	585	588
31	$SiCl_3$ asym stretch	b	565.5	578.6	588.2	22.2	3.0	$43S_{20}$, $24S_{28}$, $14S_{30}$	585	588−593
32	SiSi stretch	b	573.7	586.8	596.4	200.6	5.7	$33S_{20}$, $26S_{30}$, $13S_{27}$	593, 601?	600
33	$SiCl_3$ asym stretch	a	572.9	588.4	596.8	5.7	12.2	$78S_2$, $21S_{12}$		600
34	SiSi stretch	a	584.6	596.7	601.9	114.0	7.6	$28S_4$, $25S_{12}$, $14S_1$, $11S_3$	601−608	606
35	$SiCl_3$ asym stretch	b	578.5	593.5	602.0	330.6	0.51	$56S_{28}$, $22S_{20}$, $13S_{21}$	601−608	606
36	$SiCl_3$ asym stretch	a	578.3	592.7	606.1	134.6	2.9	$47S_{12}$, $17S_4$, $12S_3$	608−620	606−617

[a] Only values larger than 10% are listed. [b] Difference peak.

and ~490 cm^{-1} and are assigned to $\nu_{sym}(SiCl_3(b))$ and $\nu_{sym}(SiCl_2(b))$ modes, respectively. The transition from the liquid to the matrix-isolated state affects the fine structure between 580 and 620 cm^{-1} (Figure 4). No improvement of spectral resolution is observed for the residual peaks above 300 cm^{-1}, probably due to the only moderately high host-to-guest ratio required for the measurements, as well as the insensitivity of these bands to the backbone conformation.

Matrix annealing does not affect the spectral features above 300 cm^{-1} notably, and we do not show the difference spectra. Several difference peaks appear between 570 and 620 cm^{-1}. We do not attempt to assign these to individual conformers because of the expected large total number of 27 normal modes contributing in this range, most of which are predicted to have a fairly high Raman intensity. Only a positive difference peak at the highest frequency (618 cm^{-1}) is tentatively attributable to the transoid rotamer, as suggested by the calculations and guided by the analysis of the deformation mode range presented below, which will show that twisted conformers (gauche and ortho) are present in the matrices and partly convert into transoid upon annealing.

In contrast, the Raman active deformation modes below 250 cm^{-1} are predicted to be quite sensitive to the backbone conformation and there is hope to identify individual peaks of all three conformers (Tables 2−4). The highest frequency deformation mode observed (241 cm^{-1} for the liquid) is calculated to be primarily due to the transoid conformer (240.4 cm^{-1}) with a smaller contribution from ortho (238.4 cm^{-1}) and a negligible contribution from gauche (very weak; 240.6 cm^{-1}). A transoid conformer peak predicted to occur at 237.1 cm^{-1} corresponds to a b_u mode of the hypothetical planar *n*-Si_4Cl_{10} molecule and is predicted to be very weak in Raman. The next calculated vibration of the transoid conformer is displaced by ~25 cm^{-1} to lower wavenumbers (calculated, 215.1 cm^{-1}, observed in the liquid, 212 cm^{-1}). The intervening gap should only contain bands from the gauche (calculated, 224.4 and 230.5 cm^{-1}) and ortho (calculated, 226.7 and 232.2 cm^{-1}) conformers. Indeed, the Raman spectrum of liquid *n*-Si_4Cl_{10} shows a peak at 228 cm^{-1} and two shoulders at 224 and 232 cm^{-1}. These bands are absent in the solid state (Figure 2 and Table 6), while the bands at 168 cm^{-1} (see below) and 212 cm^{-1} persist.

Comparison of the residual bands of the liquid with predicted wavenumbers leads to the tentative conclusion that the Raman bands below 135 cm^{-1} and those near 189 and 199 cm^{-1} are due to all three conformers, that the band at 175 cm^{-1} should be ascribed to the transoid and gauche conformers only (the calculated values for transoid and gauche are 175.2 and 173.7 cm^{-1}, respectively) as the calculated intensity of the ortho band predicted at 174.7 cm^{-1} is almost zero, and that only the transoid conformer contributes to the band at 168 cm^{-1} (calculated, 166.4 cm^{-1}).

All these results indicate that the transoid conformer is the

TABLE 4: Vibrations of Gauche n-Si_4Cl_{10}

			calculated						observed (matrix)	
			$\tilde{\nu}$ (cm^{-1})			int IR	int Raman	MP2/6-31G*	$\tilde{\nu}$ (cm^{-1})	
mode	approximate label	sym	HF /6-31G*	B3LYP /6-31G*	MP2 /6-31G*	MP2/6-31G* (km mol^{-1})	HF/6-31G* ($Å^4$ amu^{-1})	PED (%)[a]	mid-IR	Raman
1	SiSiSiSi torsion	a	11.3	10.6	18.7	0.0	0.01	$104S_{19}$, $12S_{10}$		
2	$-SiCl_3$ torsion	b	13.6	13.9	19.3	0.0	0.00	$96S_{26}$		
3	$-SiCl_3$ torsion	a	29.8	27.1	31.1	0.0	0.05	$146S_{18}$, $72S_{10}$, $13S_{19}$		
4	SiSiSi bend	a	37.7	35.4	41.1	0.0	0.04	$41S_{10}$, $19S_{18}$		
5	SiSiSi bend	b	48.7	47.7	44.9	1.5	0.04	$80S_{35}$, $55S_{33}$		
6	$SiCl_3$ rock	b	65.1	64.7	62.3	2.1	0.04	$58S_{23}$, $52S_{24}$		
7	$SiCl_3$ rock	a	67.4	66.8	63.6	0.3	0.03	$76S_{15}$, $41S_{16}$, $25S_{17}$		
8	$SiCl_2$ twist	b	76.6	75.1	74.2	1.5	0.06	$70S_{25}$, $20S_{33}$, $17S_{24}$, $15S_{23}$, $12S_{36}$		
9	$SiCl_3$ rock	a	90.6	89.1	85.7	0.3	0.42	$61S_8$, $40S_{11}$, $23S_{17}$		
10	$SiCl_2$ twist	a	103.3	103.5	103.6	0.4	5.1	$36S_{17}$, $20S_8$		110
11	$SiCl_2$ wag	b	109.0	109.2	109.1	0.5	4.3	$17S_{36}$, $14S_{31}$, $13S_{30}$, $12S_{25}$		119
12	$SiCl_2$ wag	a	110.7	110.8	111.3	0.2	3.5	$39S_{11}$, $14S_5$, $12S_{17}$		119
13	$SiCl_2$ scissoring	b	123.8	124.7	124.8	0.0	3.6	$35S_{34}$, $11S_{31}$, $11S_{32}$		131
14	$SiCl_2$ scissoring	a	125.7	126.8	126.7	0.0	4.2	$42S_9$, $20S_6$, $16S_4$		134
15	$SiCl_2$ rock	b	138.8	140.3	138.3	2.1	0.42	$41S_{22}$, $20S_{23}$, $17S_{24}$		134
16	$SiCl_2$ rock	a	158.0	159.0	160.7	2.9	0.64	$50S_{14}$, $24S_{16}$		156, 161
17	$SiCl_3$ asym def	b	173.1	175.9	173.7	15.9	0.58	$67S_{32}$, $25S_{34}$		177
18	$SiCl_3$ asym def	a	184.7	187.2	186.7	2.0	4.7	$76S_7$		188, 190[b]
19	$SiCl_3$ asym def	b	196.0	199.3	199.2	2.0	2.6	$50S_{22}$, $11S_{23}$		199
20	$SiCl_3$ asym def	a	197.9	200.9	201.2	6.7	4.8	$30S_{14}$, $16S_9$, $15S_6$		199
21	$SiCl_3$ sym def	a	222.4	226.5	224.4	20.3	3.8	$24S_6$, $21S_{16}$, $14S_9$		226
22	$SiCl_3$ rock	b	227.1	231.2	230.5	4.1	1.3	$20S_{35}$, $19S_{34}$, $12S_{33}$		229
23	$SiCl_3$ sym def	b	238.2	241.9	240.6	68.3	0.10	$60S_{31}$, $39S_{36}$		241
24	$SiCl_2$ sym stretch	a	303.0	305.0	312.1	12.8	30.6	$21S_6$, $20S_1$, $20S_4$, $16S_3$, $13S_5$		318
25	$SiCl_3$ sym stretch	b	365.1	367.1	375.7	54.1	0.06	$53S_{27}$, $24S_{30}$, $14S_{36}$		373
26	$SiCl_3$ sym stretch	a	428.8	435.2	441.8	125.1	1.2	$54S_1$, $22S_3$, $16S_5$	444	444
27	$SiCl_2$ sym stretch	b	470.1	480.8	486.0	27.7	0.28	$73S_{29}$, $26S_{27}$	493	490
28	SiSi stretch	a	557.0	560.6	572.3	36.7	8.4	$37S_5$, $21S_3$, $20S_{13}$, $11S_4$	574	571
29	$SiCl_2$ asym stretch	a	549.5	570.5	581.9	42.3	3.8	$78S_{13}$	574−585	582
30	$SiCl_2$ asym stretch	b	555.0	571.4	582.4	14.8	4.0	$77S_{21}$, $23S_{20}$	574−585	582
31	$SiCl_3$ asym stretch	b	567.1	580.5	589.9	116.4	1.5	$76S_{28}$, $13S_{20}$	585	593
32	$SiCl_3$ asym stretch	a	569.7	585.9	593.0	14.3	4.2	$88S_{12}$, $11S_2$	593	593
33	SiSi stretch	a	575.6	589.2	597.6	62.0	9.9	$33S_2$, $20S_4$, $16S_3$, $12S_1$	593, 601?	600
34	SiSi stretch	b	580.4	589.5	600.6	178.0	3.1	$36S_{30}$, $17S_{27}$, $13S_{29}$	601−608	606
35	$SiCl_3$ asym stretch	b	577.3	595.1	605.2	381.9	3.9	$55S_{20}$, $18S_{28}$, $17S_{21}$	601−608	606−617
36	$SiCl_3$ asym stretch	a	584.6	596.8	606.5	37.9	9.9	$51S_2$, $20S_4$, $11S_3$	608−620	606−617

[a] Only values larger than 10% are listed. [b] Difference peak.

only form present in the solid. The exclusive preference for this arrangement may be due to its intrinsic stability as well as crystal packing effects and has also been observed for the tetrasilane chains n-Si_4Me_{10}[24] and $SiMe_3SiH_2SiH_2SiMe_3$.[25] Moreover, an X-ray crystal structure analysis[26] showed that solid perchloropolysilane $[SiCl_2]_n$ consists of planar all-anti SiSi backbone chains. The Raman spectrum of solid n-Si_4Cl_{10} displays very weak transoid bands near 175 and 196 cm^{-1} that would belong to the symmetry species b_u and a_u, respectively, if the conformation were anti, i.e., if the molecule assumed planar C_{2h} symmetry, in which a_u and b_u modes are not Raman allowed. This is compatible with the calculated ∼17° deviation of the backbone dihedral angle of the n-Si_4Cl_{10} chain from 180° but does not constitute an iron-clad proof since solid-state site effects (or terminal $SiCl_3$ group torsion) could in principle reduce the symmetry even if the backbone were in the planar anti conformation.

The results discussed so far leave no doubt that more than a single conformer is present in liquid n-Si_4Cl_{10} and are actually compatible with the presence of the anticipated three, but more powerful evidence is provided by the matrix isolation spectra, discussed next. In these, the fine structure between 225 and 235 cm^{-1} is better resolved and contains three bands at 226, 229, and 235 cm^{-1}. Between 130 and 165 cm^{-1}, additional bands appear at 147, 156, and 161 cm^{-1} that were hidden under the broad wing of the strong Raman band at 133 cm^{-1} in the liquid (Figure 2).

The exact details of the matrix annealing process are sensitive to experimental conditions and we describe two typical cases below. Figure 5 shows the initial spectrum of matrix-isolated n-Si_4Cl_{10} below 250 cm^{-1} as deposited at 11 K, a difference spectrum after annealing to 28 K, and a difference spectrum after annealing to 32 K relative to the spectrum obtained at 28 K (32−28 K), when the estimated host-to-guest ratio in the initial matrix was ∼200:1. Spectral measurements were always performed after recooling to 11 K. It also shows the calculated Raman spectra of the three conformers. The initial gentle annealing to 28 K leads to a small increase of peaks at ∼167 and 214 cm^{-1}, labeled t, that have already been tentatively assigned to the transoid conformer above. However, peaks labeled o increase much more dramatically while the intensity of a set of peaks labeled g drops. Clearly, at least three distinct species are present. The peak at 147 cm^{-1} (not resolved in the spectrum of the liquid) appears at a position where only the

TABLE 5: Symmetry Coordinates for *n*-Si_4Cl_{10}

species[a]	description	symmetry coordinate[b]
a_g	$SiCl_3$ sym stretch ($\nu_{sym}(SiCl_3)$)	$S_1 = r_1 + r_2 + r_3 + r_1' + r_2' + r_3'$
	$SiCl_3$ asym stretch ($\nu_{asym}(SiCl_3)$)	$S_2 = 2r_1 - r_2 - r_3 + 2r_1' - r_2' - r_3'$
	$SiCl_2$ sym stretch ($\nu_{sym}(SiCl_2)$)	$S_3 = r_4 + r_5 + r_4' + r_5'$
	SiSi stretch (ν(SiSi))	$S_4 = u + u'$
	SiSi stretch (ν(SiSi))	$S_5 = R$
	$SiCl_3$ sym def ($\delta_{sym}(SiCl_3)$)	$S_6 = \alpha_1 + \alpha_2 + \alpha_3 + \alpha_1' + \alpha_2' + \alpha_3' - \beta_1 - \beta_2 - \beta_3 - \beta_1' - \beta_2' - \beta_3'$
	$SiCl_3$ asym def ($\delta_{asym}(SiCl_3)$)	$S_7 = 2\alpha_1 - \alpha_2 - \alpha_3 + 2\alpha_1' - \alpha_2' - \alpha_3'$
	$SiCl_3$ rock ($\rho(SiCl_3)$)	$S_8 = 2\beta_1 - \beta_2 - \beta_3 + 2\beta_1' - \beta_2' - \beta_3'$
	$SiCl_2$ scissoring ($\delta(SiCl_2)$)	$S_9 = 4\epsilon - \delta_4 - \delta_5 - \gamma_4 - \gamma_5 + 4\epsilon' - \delta_4' - \delta_5' - \gamma_4' - \gamma_5'$
	SiSiSi bend (δ(SiSiSi))	$S_{10} = 5\psi - \epsilon - \delta_4 - \delta_5 - \gamma_4 - \gamma_5 + 5\psi' - \epsilon' - \delta_4' - \delta_5' - \gamma_4' - \gamma_5'$
	$SiCl_2$ wag ($\gamma(SiCl_2)$)	$S_{11} = \delta_4 + \delta_5 - \gamma_4 - \gamma_5 + \delta_4' + \delta_5' - \gamma_4' - \gamma_5'$
a_u	$SiCl_3$ asym stretch ($\nu_{asym}(SiCl_3)$)	$S_{12} = r_2 - r_3 + r_2' - r_3'$
	$SiCl_2$ asym stretch ($\nu_{asym}(SiCl_2)$)	$S_{13} = r_4 - r_5 + r_4' - r_5'$
	$SiCl_3$ asym def ($\delta_{asym}(SiCl_3)$)	$S_{14} = \alpha_2 - \alpha_3 + \alpha_2' - \alpha_3'$
	$SiCl_3$ rock ($\rho(SiCl_3)$)	$S_{15} = \beta_2 - \beta_3 + \beta_2' - \beta_3'$
	$SiCl_2$ rock ($\rho(SiCl_2)$)	$S_{16} = \delta_4 - \delta_5 + \gamma_4 - \gamma_5 + \delta_4' - \delta_5' + \gamma_4' - \gamma_5'$
	$SiCl_2$ twist ($\tau(SiCl_2)$)	$S_{17} = \delta_4 - \delta_5 - \gamma_4 + \gamma_5 + \delta_4' - \delta_5' - \gamma_4' + \gamma_5'$
	-$SiCl_3$ torsion	$S_{18} = \tau_2 + \tau_2'$
	SiSiSiSi torsion	$S_{19} = \tau$
b_g	$SiCl_3$ asym stretch ($\nu_{asym}(SiCl_3)$)	$S_{20} = r_2 - r_3 - r_2' + r_3'$
	$SiCl_2$ asym stretch ($\nu_{asym}(SiCl_2)$)	$S_{21} = r_4 - r_5 - r_4' + r_5'$
	$SiCl_3$ asym def ($\delta_{asym}(SiCl_3)$)	$S_{22} = \alpha_2 - \alpha_3 - \alpha_2' + \alpha_3'$
	$SiCl_3$ rock ($\rho(SiCl_3)$)	$S_{23} = \beta_2 - \beta_3 - \beta_2' + \beta_3'$
	$SiCl_2$ rock ($\rho(SiCl_2)$)	$S_{24} = \delta_4 - \delta_5 + \gamma_4 - \gamma_5 - \delta_4' + \delta_5' - \gamma_4' + \gamma_5'$
	$SiCl_2$ twist ($\tau(SiCl_2)$)	$S_{25} = \delta_4 - \delta_5 - \gamma_4 + \gamma_5 - \delta_4' + \delta_5' + \gamma_4' - \gamma_5'$
	$-SiCl_3$ torsion	$S_{26} = \tau_2 - \tau_2'$
b_u	$SiCl_3$ sym stretch ($\nu_{sym}(SiCl_3)$)	$S_{27} = r_1 + r_2 + r_3 - r_1' - r_2' - r_3'$
	$SiCl_3$ asym stretch ($\nu_{asym}(SiCl_3)$)	$S_{28} = 2r_1 - r_2 - r_3 - 2r_1' + r_2' + r_3'$
	$SiCl_2$ sym stretch ($\nu_{sym}(SiCl_2)$)	$S_{29} = r_4 + r_5 - r_4' - r_5'$
	SiSi stretch (ν(SiSi))	$S_{30} = u - u'$
	$SiCl_3$ sym def ($\delta_{sym}(SiCl_3)$)	$S_{31} = \alpha_1 + \alpha_2 + \alpha_3 - \alpha_1' - \alpha_2' - \alpha_3' - \beta_1 - \beta_2 - \beta_3 + \beta_1' + \beta_2' + \beta_3'$
	$SiCl_3$ asym def ($\delta_{asym}(SiCl_3)$)	$S_{32} = 2\alpha_1 - \alpha_2 - \alpha_3 - 2\alpha_1' + \alpha_2' + \alpha_3'$
	$SiCl_3$ rock ($\rho(SiCl_3)$)	$S_{33} = 2\beta_1 - \beta_2 - \beta_3 - 2\beta_1' + \beta_2' + \beta_3'$
	$SiCl_2$ scissoring ($\delta(SiCl_2)$)	$S_{34} = 4\epsilon - \delta_4 - \delta_5 - \gamma_4 - \gamma_5 - 4\epsilon' + \delta_4' + \delta_5' + \gamma_4' + \gamma_5'$
	SiSiSi bend (δ(SiSiSi))	$S_{35} = 5\psi - \epsilon - \delta_4 - \delta_5 - \gamma_4 - \gamma_5 - 5\psi' + \epsilon' + \delta_4' + \delta_5' + \gamma_4' + \gamma_5'$
	$SiCl_2$ wag ($\gamma(SiCl_2)$)	$S_{36} = \delta_4 + \delta_5 - \gamma_4 - \gamma_5 - \delta_4' - \delta_5' + \gamma_4' + \gamma_5'$

[a] Symmetry species corresponding to the hypothetical anti *n*-Si_4Cl_{10} of C_{2h} symmetry (planar backbone). The a_g and a_u blocks and the b_g and b_u blocks combine to a and b blocks, respectively, for the actual point group C_2 of the three conformers. [b] Not normalized.

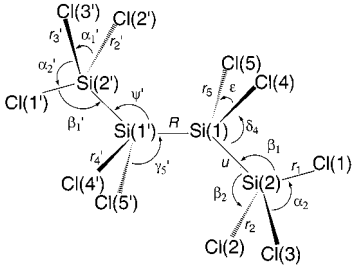

Figure 1. Definition of internal coordinates for *n*-Si_4Cl_{10}. Coordinates related by the symmetry operation C_2 are distinguished by a prime (to reduce congestion, not all symmetry-related symbols are shown).

ortho conformer is predicted to have a Raman band of substantial intensity (calculated, 148.2 cm^{-1}). The band at 161 cm^{-1} is probably assignable to the gauche rotamer (calculated, 160.7 cm^{-1}). The ab initio results thus suggest that annealing to 28 K primarily causes conversion of some fraction of the gauche conformer (negative difference peaks at 161, 223, and 230 cm^{-1}, calculated at 160.7, 224.4, and 230.5 cm^{-1}) into the ortho conformer (positive difference peaks at 147, 226, and 236 cm^{-1}, calculated at 148.2, 226.7, and 232.2 cm^{-1}). The weak peak at 156 cm^{-1} would have to be due to another gauche matrix site (see Discussion). Figure 6 illustrates that upon annealing to temperatures above 28 K the transoid peaks grow at the expense of ortho peaks, suggesting that now the ortho conformer is converted into the transoid. A positive difference peak at ~233 cm^{-1} (marked by an asterisk in Figure 5) would have to be attributed to an ortho matrix site adopted at higher annealing temperatures, since the calculations do not predict the existence of a transoid peak in this vicinity.

Figure 6 shows similar results obtained for a more dilute matrix (estimated host-to-guest ratio ~400:1). Now the initial spectrum of *n*-Si_4Cl_{10} as deposited at 11 K contains a much higher fraction of the conformer with a peak at 214 cm^{-1}, assigned as transoid, and also the qualitative annealing patterns are quite different from the case desribed first. Annealing leads to a gradual and strong increase of the 214 cm^{-1} peak already well below 28 K, while the peaks of both the gauche and ortho forms decrease. Unfortunately, a broad background in the range ~80 to ~180 cm^{-1} is superimposed on the peaks of *n*-Si_4Cl_{10} and makes a reliable interpretation of difference peaks in that spectral range difficult. This background also appears in our Raman spectrum of pure nitrogen deposited at 11 K and is believed to originate in minute amounts of fluorescent impurities in the vacuum system or in the nitrogen. Nevertheless, it is clear that the band at 177 cm^{-1} that we tentatively attribute to the transoid and gauche conformers decreases upon annealing although the gauche conformer is converting into the transoid form. This suggests that the gauche conformer contributes more intensity in this peak than the transoid conformer, in disagreement with the calculated intensities.

Mid-IR. Figure 7 shows the scaled calculated mid-IR spectra of the three conformers, the initial mid-IR spectrum of *n*-Si_4Cl_{10} as deposited at 11 K, and difference spectra after annealing to a series of temperatures. Each annealing step was followed by recooling to 11 K for spectral recording. Difference spectra

TABLE 6: Observed Vibrational Wavenumbers of Liquid, Solid and Matrix-isolated n-Si_4Cl_{10}

mid-IR		Raman		
IR (liquid)[a]	matrix-isolated	liquid	solid	matrix-isolated
90 m,b		108 vs	104 s	110 ms
		115 sh	108 s	119 ms
		133 s	117 s	131 ms
			119 s	134 s
150 sh			134 s	147 m
			137 sh	156 w
				161 w
		168 vvw	166 vw	167 m
180 vs		175 vw	175 vw	177 m
		189 m	184 m	188 s
		199 m	196 vw	199 s
207 vs		212 w	208 ms	214 ms
		224 sh		226 m
232 vs		228 w		229 mw
242 vs		232 sh		235 m
275 w		241 w	238 w	241 m
315 m		316 vvs	318 vvs	318 vvs
372 vs		372 vvw		373 vvw
440 m	444 m	441 m		444 ms
486 m	490 sh			490 vvw
	493 ms			
	574 vw,b		573 m	571 sh,w
	585 w,b	581 m	582 m	582 m
			590 m	588 m
590 vs,b	593 w	592 m		593 m
	601 sh		600 m	600 ms
	606 vvs	610 m		606 sh
	608 vvs		613 ms	
	616 w			617 ms
	620 w			

[a] IR spectra according to ref 30.

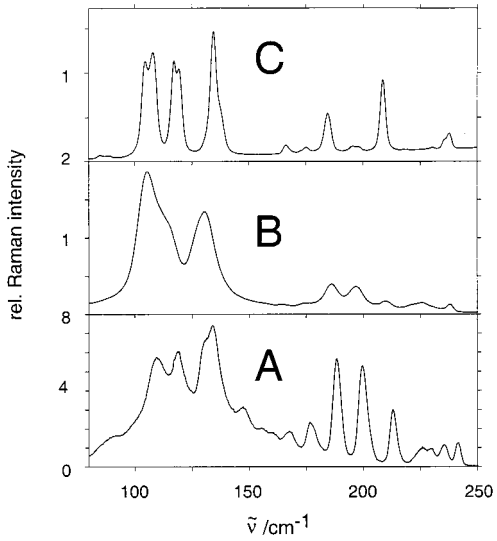

Figure 2. Raman spectra of matrix-isolated (A), liquid (B), and solid (C) n-Si_4Cl_{10}.

clearly reveal that the peak around 444 cm^{-1} gradually decreases upon gentle annealing and its maximum shifts slightly from 443.6 cm^{-1} (11 K) to 443.0 cm^{-1} (30 K). The calculations suggest that this peak is due nearly exclusively to the strongly twisted ortho and gauche conformers, since at the anti geometry (dihedral angle of 180°) this mode would be of a_g symmetry and would have no IR intensity. Its decrease upon annealing indicates that either one twisted conformer converts into another (gauche into ortho or vice versa), or one or both twisted conformers convert into the transoid form. The latter is more likely, given that the transoid conformer is calculated to be the most stable. This alternative is also strongly supported by the

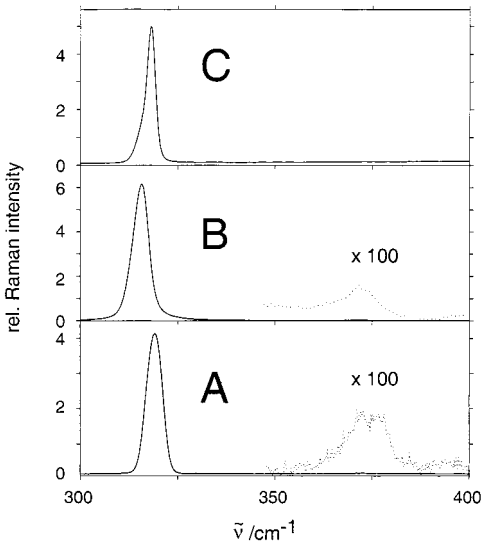

Figure 3. See caption to Figure 2.

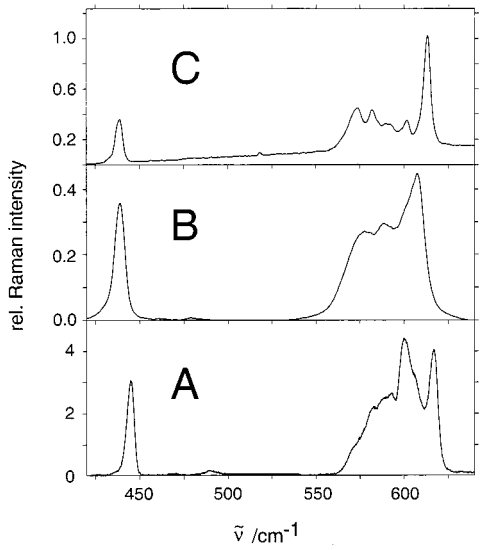

Figure 4. See caption to Figure 2.

Raman results. At annealing temperatures above 28 K the difference spectra actually produce not one but two negative peaks, at 441 and 446 cm^{-1}. It is tempting to assign these to the predicted gauche and ortho conformers, but they could also be due to two slightly different matrix sites of a single conformer.

Matrix annealing clearly affects the spectral range between 570 and 620 cm^{-1}. Calculations predict that nine fundamental vibrations originating in each of the three conformers, 27 in all, contribute to this spectral region and that they are not particularly sensitive to the backbone conformation. Guided by the calculations, and assuming that annealing converts the twisted conformers to the transoid conformer, negative difference peaks at 570, 575, 579, 591, 599, 602, 611, and 615 cm^{-1} would then be due to the sum of the strongly twisted conformers, while the strong positive difference peak at 606 cm^{-1} and the positive difference bands near 585 cm^{-1} would be ascribed to the more stable transoid conformer. There are actually three positive difference peaks at 584, 585, and 588 cm^{-1}, but only one strong transoid peak at 582.4 cm^{-1} is calculated, and the splitting is presumably due to matrix site effects.

The last important spectral range in the mid-IR occurs near 490 cm^{-1}. The difference spectra show two negative peaks at

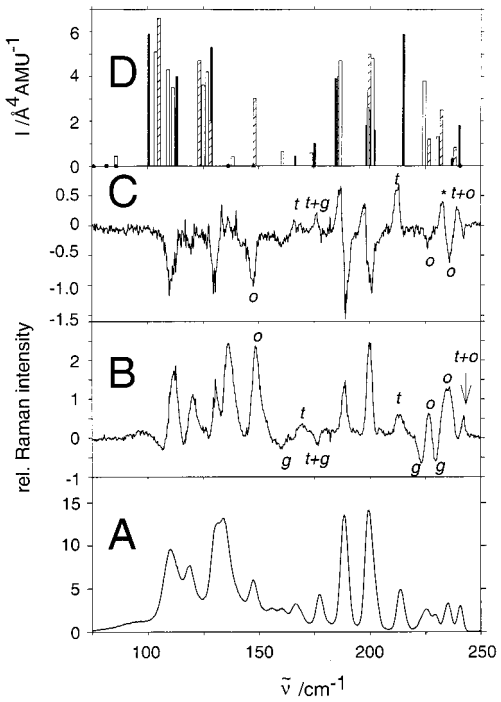

Figure 5. Raman spectrum of *n*-Si_4Cl_{10} matrix isolated in N_2 (~200:1) as deposited at 11 K (A), difference spectrum after annealing to 28 K (B), difference spectrum 32 K − 28 K (C) and calculated MP2 frequencies (scaled by 0.95) and corresponding HF intensities (D, black bars, transoid; hashed bars, ortho; white bars, gauche conformer). Note vertical scale differences. Calculated intensities smaller than 0.3 Å^4 amu^{-1} are shown as circles (transoid), triangles (ortho), and diamonds (gauche). The asterisk in panel C marks a peak tentatively attributed to a matrix site adopted by the ortho conformer at higher temperature.

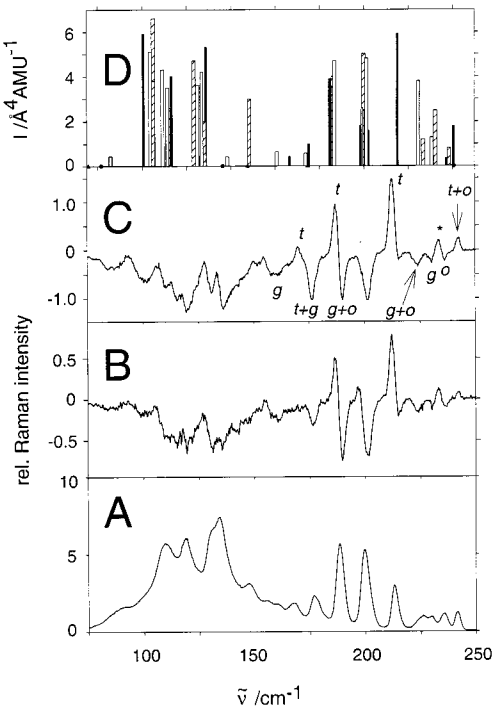

Figure 6. Raman spectrum of *n*-Si_4Cl_{10} matrix isolated in N_2 (~400:1) as deposited at 11 K (A), difference spectra after annealing to 26 K (B) and 32 K (C), and calculated MP2 frequencies (scaled by 0.95) and corresponding HF intensities (D, black bars, transoid; hashed bars, ortho; white bars, gauche conformer). Note vertical scale differences. Calculated intensities smaller than 0.3 Å^4 amu^{-1} are shown as circles (transoid), triangles (ortho), and diamonds (gauche). The asterisk in panel C marks a peak tentatively attributed to a matrix site adopted by the ortho conformer at higher temperature.

492 and 496 cm^{-1}. Assuming again that both the gauche and the ortho conformers convert into the transoid one upon annealing as deduced from the Raman results, the two negative peaks could be assigned to two strongly twisted backbone conformers or to two matrix sites of a single conformer, and a positive peak at 488 cm^{-1} could be ascribed to the transoid conformer. However, the calculations predict that the transoid conformer possesses the highest frequency $\nu_{sym}(SiCl_2(b))$ mode (491 cm^{-1}, vs 488 and 486 cm^{-1} for ortho and gauche conformers, respectively) and the calculated order then would have to be incorrect. In view of the very small observed and calculated differences among the conformers, this would not be too disturbing.

In summary, taken by themselves, the mid-IR matrix-isolation spectra strongly suggest that at least two conformers contribute to the vibrational spectra. However, unlike the Raman spectra, they provide no more than a hint of evidence for the existence of two different twisted backbone conformations, as the observed effects could equally well be due to a multitude of matrix sites. Since most assignments of difference peaks in the spectrally crowded regions of the mid-IR to individual conformers are unsafe and difficult, we have refrained from including these difference peaks in Tables 2−4, and label several assignments in the mid-IR by a question mark.

Singular Value Decomposition of the Observed Spectra. Although the above qualitative analysis of the annealing results is strongly suggestive, it does not definitely prove that three and only three spectrally distinct species are present in the matrices. Nonsubjective procedures for such a determination are, however, available. Singular value decomposition (SVD)[22] and the closely related principal component analysis (PCA)[27] have been used extensively for the determination of the number of independent spectrally active components present in a system. We have used the SVD method to prove that three principal components are present in the matrices. Comparison with calculated spectra then identifies them as the transoid, ortho, and gauche conformers beyond reasonable doubt.

The general assumption of SVD is that the observed spectra are linear combinations of the spectra of the pure components. The experimental data matrix **A** consists of elements A_{ij} where the row index *i* refers to a wavelength and the column index *j* denotes a particular observed mixture. The mixtures were obained by matrix annealing to various temperatures followed by cooling to 11 K before spectra were taken. The SVD algorithm finds the decomposition $\mathbf{A} = \mathbf{USV}^T$, where **U** and **V** are orthogonal matrices and **S** is a diagonal matrix containing the singular values s_i along the diagonal in descending order of size. The column vectors $\boldsymbol{u}_i$ of the matrix **U** are referred to as the basis spectra, and they are mutually orthogonal. The number *r* of components present in a system equals the effective rank of the data matrix **A**. This is the number of the first *r* diagonal elements of the matrix **S** and first *r* columns of the matrices **U** and **V** that are required to calculate a matrix $\mathbf{A}_r$ that is indistinguishable from the observed data matrix **A** within a given experimental error, i.e., $\mathbf{A} \approx \mathbf{A}_r = \mathbf{U}_r\mathbf{S}_r\mathbf{V}_r^T$. The size of the singular value s_i as well as the autocorrelation c_i of the basis spectrum $\boldsymbol{u}_i$ defined by Shrager and co-workers[28] are usually used as additional criteria to decide whether a basis spectrum represents noise or contains significant spectral information. Basis spectra with *c* values smaller than ~0.8 are usually regarded as pure noise.

Figures 8−10 show the basis spectra corresponding to the four largest singular values obtained by SVD analysis of a series of our annealed mid-IR matrix-isolation spectra. The three

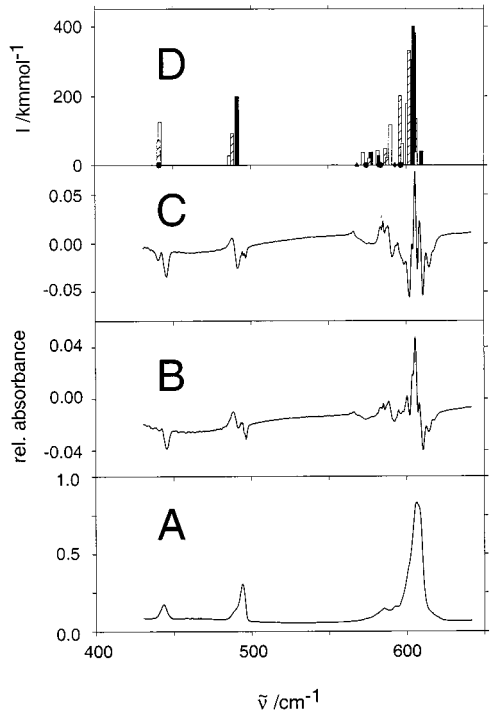

Figure 7. Mid-IR matrix-isolation spectrum of n-Si_4Cl_{10} in N_2 as deposited at 11 K (A), difference spectra after annealing to 28 K (B) and 32 K (C) and calculated MP2 frequencies (scaled by 0.95) and intensities (D, black bars, transoid; hashed bars, ortho; white bars, gauche conformer). Note vertical scale differences. Calculated intensities smaller than 20 km mol^{-1} are shown as circles (transoid), triangles (ortho), and diamonds (gauche).

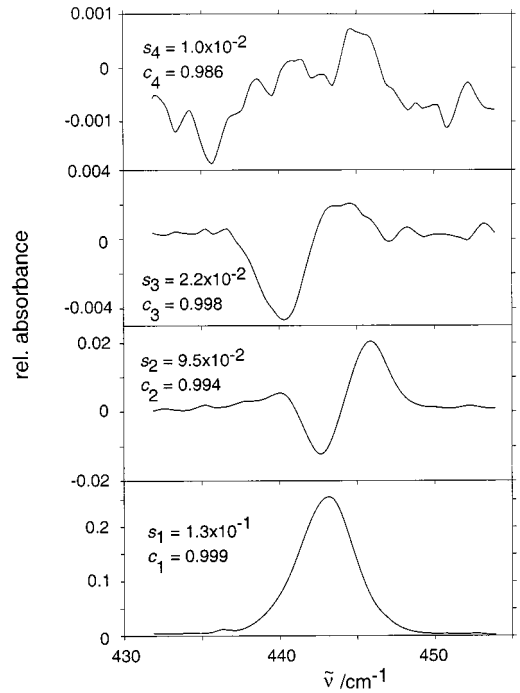

Figure 8. Singular value decomposition: mid-IR basis spectra corresponding to the four largest singular values s_i.

spectral ranges in the mid-IR (the single peak at 444 cm^{-1}, the region around 490 cm^{-1} and the range from 570 to 620 cm^{-1}) have been analyzed individually. Inspection of the s_i values obtained by the SVD procedure suggests that only two basis spectra are required to model the peak at 444 cm^{-1}, in agreement with our proposal that only the gauche and ortho conformers contribute to this band. In contrast, three basis spectra are

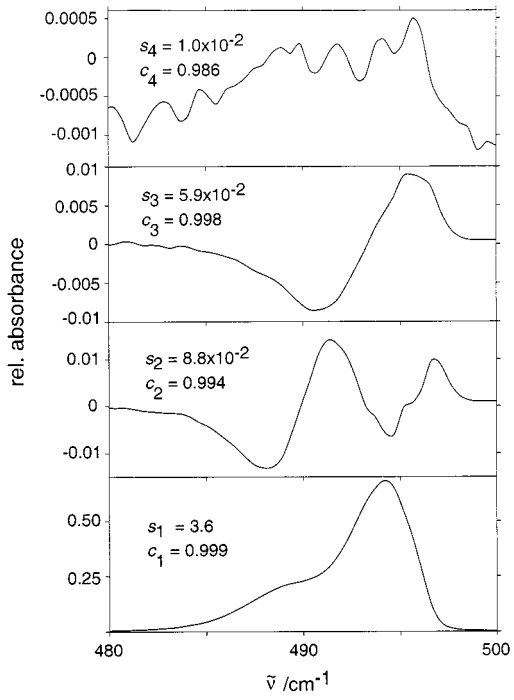

Figure 9. See caption to Figure 8.

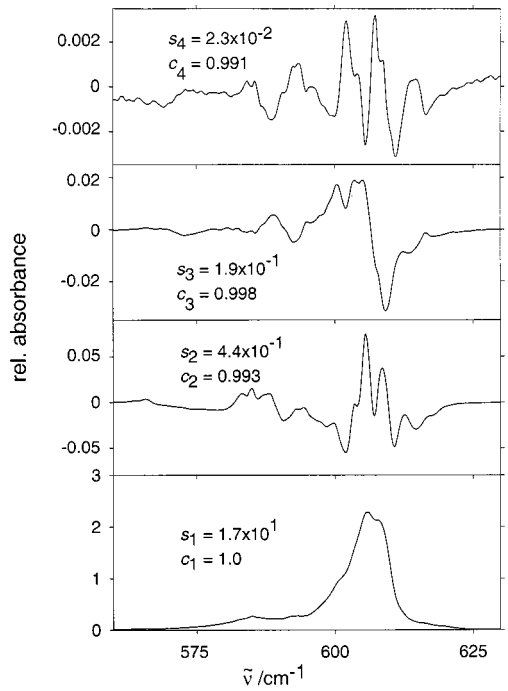

Figure 10. See caption to Figure 8.

necessary to reproduce the other two spectral regions within experimental error. Although it is tempting to identify these as the transoid, ortho, and gauche conformers, an accidental interplay of site effects perhaps might be responsible for the observed effects.

A similar SVD analysis of the Raman spectra of matrix-isolated n-Si_4Cl_{10} below 300 cm^{-1} leaves no doubt. Figure 11 depicts the first four basis spectra obtained by SVD analysis of the Raman spectra. Three components are clearly present, corresponding to the singular values $s_1 = 2.0 \times 10^2$, $s_2 = 5.8$ and $s_3 = 2.0$. The fourth basis spectrum ($s_4 = 9.3 \times 10^{-1}$) represents almost pure noise ($c_4 = 0.765$) and is not needed to reproduce the experimental data within the error limits. We conclude that there definitely are three distinct contributors to

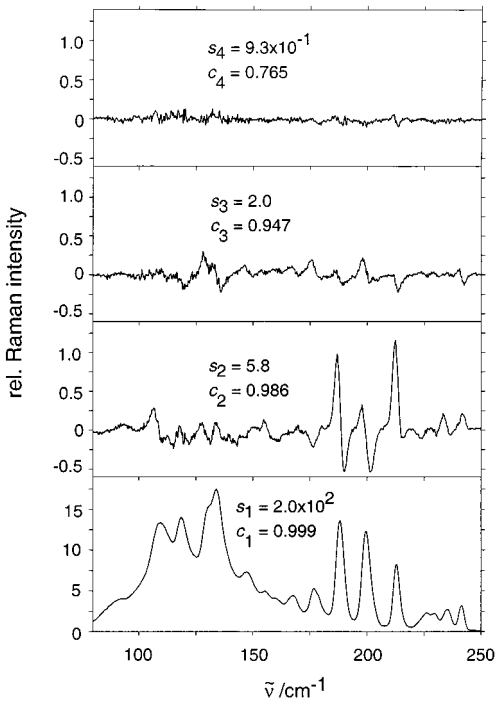

Figure 11. Singular value decomposition: Raman basis spectra corresponding to the four largest singular values s_i.

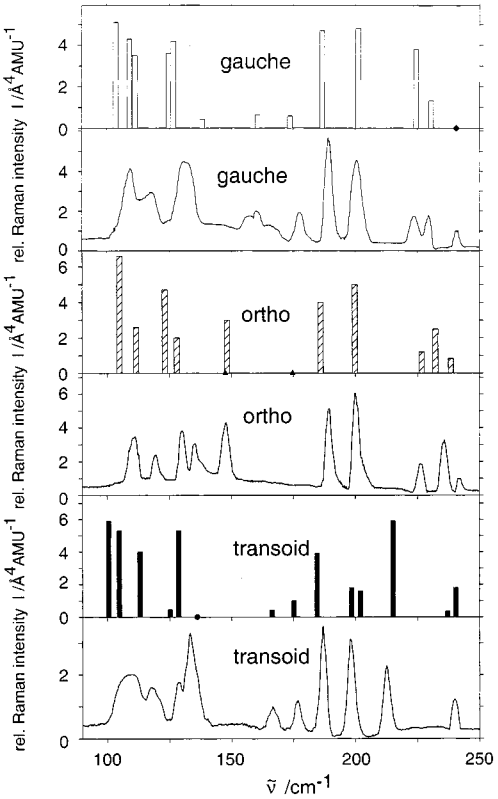

Figure 12. Pure component Raman spectra (<250 cm^{-1}) obtained from linear combinations of SVD basis spectra, and calculated MP2 frequencies (scaled by 0.95) and corresponding HF intensities. Note vertical scale differences. Calculated intensities that are smaller than 0.3 Å^4 amu^{-1} are shown as circles (transoid), triangles (ortho), and diamonds (gauche).

the mixture, as anticipated. There is no indication that a larger number of contributors exists.

To obtain the best approximation to the spectra of the pure transoid, ortho, and gauche conformers from the orthogonal basis spectra, we form their linear combinations that have only positive values over the whole spectral range and in which peaks due to two of the conformers are eliminated. The above qualitative analysis suggested that the bands attributed to a single conformer alone are those at 167 and 214 cm^{-1} (transoid), 147 and 235 cm^{-1} (ortho), and 161 and 229 cm^{-1} (gauche). Using this information to guide the formulation of nonorthogonal linear combinations of the three basis spectra, we obtain the pure conformer spectra shown in Figure 12. They agree quite well with the spectra predicted by theory. The relative band intensities in the spectrum of the matrix-isolated transoid conformer differ from the spectrum of solid *n*-Si_4Cl_{10}, which is presumably also transoid, most likely due to solid-state effects on the backbone dihedral angle. In particular, in the spectrum of the solid, the peak at 199 cm^{-1} is much weaker relative to the peaks at 188 and 214 cm^{-1} than it is in the matrix spectrum or than calculated. This peak is assigned to a superposition of an a_u and a b_u vibration, both forbidden in the planar form ($\phi = 180°$), and the curious intensity variation is most naturally accounted for by postulating that in the solid ϕ is much closer to 180° than in the matrix-isolated species, and perhaps even equal to 180°, as is the case in the $[SiCl_2]_n$ polymer.[26]

Since the annealing itself as well as the possible presence of different sites changes the spectral positions of peaks slightly, it is very difficult to form linear combinations of basis spectra such that a certain peak disappears completely into a flat baseline. Usually, derivative-shaped "wiggles" remain. The three pure component spectra shown in Figure 12 have been cleaned up by introducing very small shifts of peaks in the basis spectra before forming the linear combinations. The SVD analysis suffers from the fact that the spectral changes due to annealing are small, making the basis spectra corresponding to s_2 and s_3 somewhat noisy.[29]

The SVD analysis of the three Raman ranges corresponding to stretching modes (near 316 cm^{-1}, near 442 cm^{-1} and from 580 to 620 cm^{-1}) in each case arrived at the conclusion that the spectra can be well described as linear combinations of the spectra of two components. This is compatible with the theoretical prediction that the Raman spectra of the three conformers do not differ significantly from each other in the stretching mode regions.

Discussion

The Transoid, Ortho, and Gauche Conformers of *n*-Si_4Cl_{10}. Whereas the mid-IR matrix-isolation spectrum of *n*-Si_4Cl_{10} does not provide conclusive evidence for or against the existence of a third backbone conformer (ortho), the Raman matrix-isolation spectra leave no doubt that three backbone conformers of *n*-Si_4Cl_{10} are indeed trapped in nitrogen matrices deposited at 11 K. Although experimental evidence for the existence of three conformers in C_4F_{10} chains has been available,[2,3] to our best knowledge, this is the first such evidence for tetrasilane chains. The observed peak positions agree almost perfectly with the scaled calculated MP2/6-31G* frequencies, permitting a safe assignment to the calculated individual conformers, transoid, ortho, and gauche. It seems extremely unlikely that the Raman peaks that we attributed to the ortho conformer instead could correspond to another gauche matrix site and that the annealing accidentally leads to an increase of peaks attributed to the ortho conformer and a simultaneous decrease of peaks ascribed to the gauche conformer (see Figure 5). In particular, the three Raman peaks of matrix-isolated *n*-Si_4Cl_{10} near 226 cm^{-1} (assigned to ortho and gauche), 229 cm^{-1} (assigned to gauche), and 235 cm^{-1} (ascribed to ortho) have counterparts at 224, 228,

and 232 cm^{-1} in the spectrum of the liquid and thus are definitely not due to matrix sites.

The annealing results leave no doubt that at least in some matrix environments the transoid conformer of n-Si_4Cl_{10} is the most stable of the three, and that the ortho form is more stable than the gauche conformer. This stability order agrees with the HF/6-31G* and B3LYP/6-31G* results for isolated molecules, but not with the MP2(FC)/6-31G* result. Of course, the calculated energy differences are small and differential environmental effects on stability need not be negligible.

The host-to-guest matrix-isolation ratio and possibly other experimental details such as deposition rate have two significant effects on the results. First, they determine the initially deposited conformer ratio, which also is a function of deposition temperature, and second, they affect the kinetics of conformer interconversion upon annealing. As the host-to-guest ratio increases, the transoid form increasingly dominates the initial composition. We propose that this is due to slower cooling of the deposited guest molecules in nearly pure nitrogen compared to nitrogen contaminated with a significant amount of the guest molecules, which are effective at randomizing the energy of molecular vibrations into heat.

The observed effect of the matrix-isolation ratio on the rate of the interconversion of the conformers in the matrix suggests that the effective viscosity of the matrix increases as the guest concentration grows, and this appears reasonable. It was particularly fortunate that we found experimental conditions with relatively high guest concentrations where up to annealing temperatures of 28 K the gauche conformer is primarily converted into the ortho conformer, and this is only converted to the transoid conformer at higher temperatures. One could hardly ask for a more convincing demonstration of the presence of three species. Moreover, this result demonstrates that in this highly viscous medium the gauche → ortho transformation is easier than the ortho → transoid or gauche → transoid interconversions, as would be anticipated from the dihedral angle changes involved.

However, all of our studies show that even matrices annealed to 32 K contain substantial amounts of remaining twisted backbone conformers and that the transformation process of twisted conformers into the transoid structure is far from complete. A similar observation was made for the tetrasilane chain n-Si_4Me_{10} in xenon matrix,[5] where annealing led only to partial conversion of the gauche into the transoid form (at the time called anti). Clearly, the distribution of activation energies for conformer interconversion as a function of detailed matrix environment is very wide. In contrast, in matrix isolation studies of n-C_4F_{10} in N_2 matrix[2,3] the ortho conformer disappeared quantitatively after annealing to 16 K and the gauche → transoid rearrangement was complete after annealing to 25 K. Apparently, the interconversion of backone conformers in matrices is much more demanding for the larger tetrasilane backbones than the smaller perfluorinated butanes. The more quantitative aspects of conformer interconversion induced by matrix annealing clearly leave much room for further exploration.

Vibrational Assignments and Calculated Potential Energy Distributions. Some time ago, Hassler and co-workers reported the results of a normal-coordinate analysis on n-Si_4Cl_{10} using a set of spectroscopic force field parameters that were fitted to represent the observed frequencies.[30] Their analysis was based on the assumption that only a single anti conformer of C_{2h} symmetry contributed to the observed spectra. Observed bands that did not quite obey the mutual rule of exclusion imposed by the point group C_{2h} were attributed to impurities rather than to the occurrence of rotational isomerism. We now have at our disposal the results of reasonable ab initio calculations and a set of fairly well-resolved mid-IR and Raman matrix-isolation spectra, and some of the vibrational assignments we make for n-Si_4Cl_{10} differ from those reported earlier.[30] We next briefly discuss the assignments and some characteristics of the potential energy distributions (PEDs).

Because of the similar masses of Si and Cl atoms strong vibrational mixing between various types of motion must be anticipated. Indeed, the calculated PED values (Tables 2−4) reveal that only a few of the calculated normal modes are dominated by a single symmetry coordinate. Most represent mixtures of two, three, or even a larger number of dominant symmetry coordinates, and a few symmetry coordinates are the dominant contribution in two different normal modes. The description of normal modes by a single coordinate is thus highly approximate and merely helps with labeling rather than permitting an exact characterization of the vibrational modes.

The spectrum of n-Si_4Cl_{10} will be divided into regions dominated by SiSi and asymmetric SiCl stretches (calculated, 568.6−609.9 cm^{-1}), symmetric SiCl stretches (calculated, 312.1−491.2 cm^{-1}), a range of deformation modes (calculated, 36.6−240.6 cm^{-1}), and torsional vibrations around the SiSi bonds (calculated, 14.8−31.1 cm^{-1}). In the following section, when we refer to observed frequencies, we always mean matrix-isolated n-Si_4Cl_{10}.

SiSi and Asymmetric SiCl Stretches. The three SiSi stretches span the irreducible representations 2a + b ($2a_g + b_u$ in the hypothetical planar anti structure). The calculated PED values show that the SiCl and SiSi stretching modes are strongly mixed. As a consequence the latter are blue-shifted from values near 450 cm^{-1} observed in methylated oligosilanes or polysilanes toward values above 550 cm^{-1} in n-Si_4Cl_{10}. The highest experimental value of ν(SiSi) is perhaps that reported by Höfler et al.[31] in the Raman spectrum of Si_2Cl_6 (624 cm^{-1}), where a normal-coordinate analysis employing spectroscopic force constants showed a strong mixing between the symmetry coordinates $\nu_{sym}(SiCl_3)$ and ν(SiSi), with the latter dominating the 624 cm^{-1} vibration. This result was confirmed very recently by ab initio calculations.[32] For the three conformers of n-Si_4Cl_{10} the highest SiSi stretching mode is predicted at 609.9 (transoid, PED dominated by S_4), 601.9 (ortho, PED dominated by S_4), and 600.6 cm^{-1} (gauche, PED dominated by S_{30}) and is observed near 616 and 606 cm^{-1}, respectively. The stretching mode of the central SiSi bond ν(SiSi(a,a_g)) is predicted at 574.5 (transoid), 568.6 (ortho), and 572.3 cm^{-1} (gauche) and is observed near 571 cm^{-1} in the Raman spectrum. This normal mode is calculated to contain significant contributions from $\nu_{asym}(SiCl_2(S_{13}))$, and $\nu_{sym}(SiCl_2(S_3))$, and S_{13} actually dominates the PED for the ortho conformer (PED: 35 S_{13}, 31 S_5, 21 S_3). The frequency of the SiSi mode of symmetry b(b_u) is sensitive to the backbone conformation and is predicted at 577.5 (transoid), 596.4 (ortho), and 600.6 cm^{-1} (gauche). Again, the labeling of these modes as ν(SiSi) is highly approximate since for the transoid form, νS(Si(b,b_u)) contains strong admixtures from $\nu_{asym}(SiCl_3(S_{28}))$ and $\nu_{asym}(SiCl_2(S_{21}))$, and for the ortho form, $\nu_{asym}(SiCl_3(S_{20}))$ is the dominant symmetry coordinate.

Asymmetric SiCl stretches can be divided into $\nu_{asym}(SiCl_3)$ modes spanning the irreducible representations 2a + 2b ($a_g + a_u + b_g + b_u$) and $\nu_{asym}(SiCl_2)$ modes transforming as a + b ($a_u + b_g$). These modes are not particularly sensitive to the backbone conformations and possess reasonably simple potential energy distributions, such that their description by a single symmetry coordinate is justified, though far from perfect. These modes

are observed in the range from 570 to 617 cm^{-1} and need not be discussed in detail.

Symmetric SiCl Stretches. The symmetric SiCl stretches can be divided into $\nu_{sym}(SiCl_2)$ stretches spanning the irreducible representations a + b ($a_g + b_u$) and $\nu_{sym}(SiCl_3)$ modes transforming as a + b ($a_g + b_u$). These modes are also predicted to be relatively insensitive to backbone conformation. The $\nu_{sym}(SiCl_2(a,a_g))$ and two $\nu_{sym}(SiCl_3)$ modes are observed at 318, 373, and 444 cm^{-1}, respectively. The $\nu_{sym}(SiCl_2(a,a_g))$ mode has strong contributions from $\delta_{sym}(SiCl_3(a,a_g))$, which actually dominates this mode in the gauche and ortho conformers. The remaining $\nu_{sym}(SiCl_2(b,b_u))$ mode is predicted at 491.2 (transoid), 488.1 (ortho), and 486.0 cm^{-1} (gauche). The observed values are 488 cm^{-1} (difference peak) for transoid and 493 cm^{-1} for gauche and ortho, as suggested by matrix annealing.

Deformation Modes. ClSiCl deformations appear below 250 cm^{-1}. They are predicted to have a fairly high Raman intensity and some are calculated to vary substantially with the SiSiSiSi dihedral angle. The 18 modes can be subdivided into two symmetric $SiCl_3$ deformations, four asymmetric $SiCl_3$ deformations, four $SiCl_3$ rocks, and eight $SiCl_2$ deformations (two scissors, two wags, two twists, and two rocks). As already mentioned earlier, most of these modes are heavily mixed and any labeling is highly approximate. The two $\delta_{sym}(SiCl_3)$ modes belong to the irreducible representations a + b ($a_g + b_u$). The a transitions are calculated to occur at 240.4, 232.2, and 224.4 cm^{-1} and are observed at 241, 235, and 226 cm^{-1} in the transoid, ortho, and gauche conformers, respectively. The corresponding b transitions are predicted at 202.0, 238.4, and 240.6 cm^{-1} and are observed at 199 (transoid) and 241 cm^{-1} (ortho and gauche).

The four asymmetric $SiCl_3$ deformations transform as 2a + 2b ($a_g + a_u + b_g + b_u$). For the transoid conformer these are predicted to occur at 166.4 (b,b_g), 175.2 (b,b_u), 184.6 (a,a_g), and 198.5 cm^{-1} (a_u,a) and they are readily observed at 167, 177, 188, and 199 cm^{-1}, respectively. The $\delta_{asym}(SiCl_3)$ modes are predicted to be virtually identical for gauche and ortho conformers. The observed values are 177 (b), 188 (a), and 199 (a + b) cm^{-1}.

The discussion of the remaining ClSiCl deformations is not straightforward as the frequencies of the modes labeled by the same symmetry coordinate can differ quite strongly due to the complicated vibrational coupling patterns. For example, for the ortho conformer the four $SiCl_3$ rocks that are predicted to occur below 90 cm^{-1} have weak intensities and have not been observed, while for the gauche conformer, one $\rho(SiCl_3)$ mode is calculated to appear at 230.5 cm^{-1} and is observed at 229 cm^{-1}. The $\rho(SiCl_2(a))$ mode is fairly well defined for the twisted backbone conformers, in that the potential energy distributions are similar (ortho: 37 S_{14}, 25 S_{16}, 13 S_9, 13 S_{15}; and gauche: 50 S_{14}, 25 S_{16}). This mode is sensitive to the backbone conformation and the calculated values are 148.2 (ortho) and 160.7 cm^{-1} (gauche). These modes are observed at 147 and 161 cm^{-1}. An additional band at 156 cm^{-1} is very likely due to the $\rho(SiCl_2(a))$ mode of another gauche matrix site, perhaps one that has a backbone dihedral angle a little closer to that of the ortho conformer.

SiSiSi bending modes are predicted to lie below 50 cm^{-1}. They have not been observed in the present study.

Torsional Vibrations. Torsional vibrations around the SiSi bonds are calculated to have frequencies below 35 cm^{-1}. Not surprisingly, the torsion around the central SiSi bond is predicted to have the smallest wavenumber, about 15 cm^{-1}. All torsional modes of *n*-Si_4Cl_{10} eluded observation.

Conclusions

Our conclusions can be summarized as follows:

(i) As expected from prior general arguments,[7] all three levels of theory used predict the existence of three conformers of Si_4Cl_{10} (transoid, ortho, and gauche) of comparable energies.

(ii) The three conformers have been observed by vibrational spectroscopy on a matrix-isolated sample of Si_4Cl_{10}. Their Raman and IR spectra agree very well with theoretical predictions.

(iii) At least in some and possibly in all sites in the matrix, the stability of the conformers increases in the order gauche, ortho, transoid.

(iv) Neat solid Si_4Cl_{10} contains only the transoid conformer, at a geometry that appears to be closer to the planar anti form than is the case for the matrix-isolated transoid species. This may be due to crystal packing forces (note that the polymer, $[SiCl_2]_n$, is planar all-anti in the solid form[26]).

Acknowledgment. This work was supported by a grant from the USARO (DAAG55-98-10310) and by an NSF instrumentation grant (CHE-9709195). R.Z. is grateful to the Austrian FWF for a postdoctoral fellowship. The authors thank Dr. John W. Downing for help with computations and for writing a computer program for SVD analysis.

References and Notes

(1) For example: Morokuma, K. *J. Chem. Phys.* **1971**, *54*, 962. Welsh, W. J.; Johnson, W. D. *Macromolecules* **1990**, *23*, 1882.

(2) Albinsson, B.; Michl, J. *J. Am. Chem. Soc.* **1995**, *117*, 6378.

(3) Albinsson, B.; Michl, J. *J. Phys. Chem.* **1996**, *100*, 3418.

(4) Teramae, H.; Michl, J. *Mol. Cryst. Liq. Cryst.* **1994**, *256*, 149.

(5) Albinsson, B.; Teramae, H.; Downing, J. W.; Michl, J. *Chem. Eur. J.* **1996**, *2*, 529.

(6) Smith, G. D.; Jaffe, R. L.; Yoon, D. Y. *Macromolecules* **1994**, *27*, 3166.

(7) Neumann, F.; Teramae, H.; Downing, J. W.; Michl, J. *J. Am. Chem. Soc.* **1998**, *120*, 573.

(8) Fogarty, H. A.; Ottosson, C. H.; Michl, J. *J. Mol. Struct.* (*THEOCHEM*), in press.

(9) Fogarty, H. A.; Ottosson, C. H.; Michl, J. *J. Mol. Struct.*, in press.

(10) Michl, J.; West, R. In *Silicon-Containing Polymers: The Science and Technology of their Synthesis and Applications*; Jones, R. G., Ando, W., Chojnowski, J., Eds.; Kluwer Academic Publishers: Dordrecht, The Netherlands, in press.

(11) Imhof, R.; Antic, D.; David, D. E.; Michl, J. *J. Phys. Chem. A* **1997**, *101*, 4579.

(12) Imhof, R.; Teramae, H.; Michl, J. *Chem. Phys. Lett.* **1997**, *270*, 500.

(13) Neumann, F.; Michl, J. In *The Encyclopedia of Computational Chemistry*; Schleyer, P. v. R., Allinger, N. L., Clark, T., Gasteiger, J., Kollman, P. A., Schaefer, H. F., III, Schreiner, P. R., Eds.; Wiley: Chichester, England, 1998; Vol. 1, p 556.

(14) Crespo, R.; Teramae, H.; Antic, D.; Michl, J. *Chem. Phys.* **1999**, *244*, 203.

(15) Albinsson, B.; Antic, D.; Neumann, F.; Michl, J. *J. Phys. Chem. A* **1999**, *103*, 2184.

(16) Belyakov, A. V.; Haaland, A.; Shorokhov, D. J.; West, R. *J. Organomet. Chem.*, in press.

(17) Raml, W.; Hengge, E. *Z. Naturforsch.* **1979**, *34b*, 1457.

(18) Kovar, D. Thesis, University of Technology, Graz, 1978.

(19) *Gaussian 94*, Revision E.1; Frisch, M. J.; Trucks, G. W.; Schlegel, H. B.; Gill, P. M. W.; Johnson, B. G.; Robb, M. A.; Cheeseman, J. R.; Keith, T.; Petersson, G. A.; Montgomery, J. A.; Raghavachari, K.; Al-Laham, M. A.; Zakrzewski, V. G.; Ortiz, J. V.; Foresman, J. B.; Cioslowski, J.; Stefanov, B. B.; Nanayakkara, A.; Challacombe, M.; Peng, C. Y.; Ayala, P. Y.; Chen, W.; Wong, M. W.; Andres, J. L.; Replogle, E. S.; Gomperts, R.; Martin, R. L.; Fox, D. J.; Binkley, J. S.; Defrees, D. J.; Baker, J.; Stewart, J. P.; Head-Gordon, M.; Gonzalez, C.; Pople, J. A. Gaussian, Inc.: Pittsburgh, PA, 1995.

(20) Hedberg, L.; Mills, I. A. *J. Mol. Spectrosc.* **1993**, *160*, 117.

(21) Wilson, E. B., Jr.; Decius, J. C.; Cross, P. C. *Molecular Vibrations*; McGraw-Hill: New York, 1955.

(22) For example: Henry, E. R.; Hofrichter, J. *J. Methods Enzymol*. **1992**, *210*, 129. Wallace-Williams, S. E.; Møller, S.; Goldbeck, R. A.; Hanson, K. M.; Lewis, J. W.; Yee, W. A.; Kliger, D. S. *J. Phys. Chem.* **1993**, *97*, 9587.

(23) Anderson, E.: Bai, Z.; Bischof, C.; Demmel, J.; Dongarra, J.; Du Croz, J.; Greenbaum, A.; Hammarling, S.; McKenney, A.; Ostrouchov, S.; Sorensen, D. *Lapack Users' Guide*, 2nd ed.; 1994.

(24) Ernst, C. A.; Allred, A. L.; Ratner, M. A. *J. Organomet. Chem.* **1979**, *178*, 119.

(25) Zink, R.; Tekautz, G.; Kleewein, A.; Hassler, K., unpublished results.

(26) Koe, J. R.; Powell, D. R.; Buffy, J. J.; Hayase, S.; West, R. *Angew. Chem.* **1998**, *110*, 1514.

(27) For example: Malinowski, E. R.; Howery, D. G. *Factor Analysis in Chemistry*; John Wiley & Sons: New York, 1980. Saltiel, J.; Sears, D. F. Jr.; Choi, J.-O.; Sun, Y.-P.; Eaker, D. W. *J. Phys. Chem.* **1994**, *98*, 35. Lawton, W. H.; Sylvestre, E. A. *Technometrics* **1971**, *13*, 617.

(28) Shrager, R. I. *Chemom. Intell. Lab. Syst.* **1986**, *1*, 59. Shrager, R. I.; Hendler, R. W. *Anal. Chem.* **1982**, *54*, 1147.

(29) An attempt to introduce larger differences by starting with a matrix deposited from hot (50−200 °C) gas failed because of sample decomposition at these higher temperatures, apparently catalyzed by one of the materials inside the oven.

(30) Hassler, K.; Hengge, E.; Raml, W. *Monatsh. Chem.* **1980**, *111*, 581.

(31) Höfler, F.; Sawodny, W.; Hengge, E. *Spectrochim. Acta* **1970**, *26A*, 819.

(32) Ernst, M.; Schenzel, K.; Jähn, A.; Köll, W.; Hassler, K. *J. Raman Spectrosc.* **1997**, *28*, 589.